Article

Development of a Novel Fabrication Process for Application in Glass Gas Electron Multiplier Detectors

Xiaomeng Wu [1,2], **Xilei Sun** [3], **Liqiang Cao** [1,*] **and Qidong Wang** [1,*]

[1] Institute of Microelectronics of the Chinese Academy of Sciences, Beijing 100029, China
[2] School of Integrated Circuits, University of Chinese Academy of Sciences, Beijing 101408, China
[3] State Key Laboratory of Particle Detection and Electronics, Institute of High Energy Physics,
    Chinese Academy of Sciences, Beijing 100049, China
* Correspondence: caoliqiang@ime.ac.cn (L.C.); wangqidong@ime.ac.cn (Q.W.)

Abstract: Gas electron multipliers (GEMs) have been widely used for particle collection and signal amplification. Because of the advantages of glass, such as high hardness, aging resistance, and dielectric strength, research into its application as a substrate material in GEM design and process has attracted extensive attention in recent years. This paper compares two commonly used glass GEM structural designs and shows that the optical transparency of the hexagonal symmetric structure is superior to that of the rectangle structure. An electric field model is developed to characterize the negative correlation between the hole diameter and the electric field strength. The structure of glass GEM is designed according to the feasibility of the process. A new process method of surface metal patterning using hole filling to form a mask is proposed, which can meet the high alignment and shaping requirements of the perfect match between the opening of metal layer and the aperture shape of the substrate. Combined with the advanced laser hole modification process, a glass GEM sample with a hole diameter of 70 μm, a spacing of 140 μm, a substrate thickness of 240 μm, and a metal thickness of 13 μm is obtained. Finally, particle trajectories, avalanche region coverage, and electron energy are discussed based on the prototype structure.

Keywords: gas electron multiplier (GEM); glass; transparency; process; hexagonally symmetrical structure; electric field

1. Introduction

Since the invention of the first GEM [1] by Fabio Sauli at CERN in 1997, the structure consisting of two layers of metal, a supporting dielectric (used to be a Kapton foil), and through-holes has been widely used in X-ray [2–5], charge particle detection [6–8], and imaging [9]. By loading a voltage difference between the upper and lower surfaces, the GEM is able to generate strong electric fields. Electrons or other particles enter the holes from the drift region above the GEM, gaining enough energy and then colliding with the gas molecules. When the bias voltage is large enough, an avalanche occurs. Then, the particles are collected by the receiver at the bottom or they enter the next stage of the gas electron amplifier for another multiplication reaction.

Early GEM detectors were fabricated by the photolithographic process using 5 μm copper on both surfaces of a 50 μm thick Kapton foil with double conical hole arrays. This structure can achieve a significant gain (typically up to around 100 [10]), but the gain decreases over time, because particles tend to accumulate on the surface and the insulating wall. In addition, this structure is difficult to apply in a large area due to the limitation of stiffness and the thickness of the foil. In 2004, Chechik [11] proposed the concept of thick GEM with structural parameters 5–20 times larger (can be larger than 600×600 mm^2) and a higher gain (can be more than 10^5) than those of conventional GEM, which not only requires much less technology, accuracy, and equipment, but is also stronger and more durable than conventional GEM, while the cost of fabrication and the environmental

requirements are greatly reduced. Glass is a preferred choice for thick GEMs compared with PCBs for stiffness in large scale fabrication, ageing resistance in long-term operation, and high dielectric strength in high-voltage applications. In addition, in applications such as the detection of high-energy particles (such as neutrinos and dark matter) and space flight, GEM detectors are strictly required to have low background levels of radioactivity and low outgassing rates. As was measured in [12–15], compared with other GEM substrate materials such as polyimides, epoxies, and polyimide films, fused silica glass (may also be called "quartz" in some papers) contains a very small amount of radioactive substances, represented by ^{232}Th, ^{238}U, and ^{40}K.

Over the past few decades, researchers have performed extensive numerical calculations and simulations on how to increase the gains of GEMs. The relationship among voltage, thickness, gas composition, and gain was analyzed [11,16–19]. The discharge was studied [19–23] and the cascade method was proposed to achieve maximum efficiency [24–27]. However, most studies focus on how to increase the absolute gain (G_{abs}) of GEM or the effective gain (G_{eff}) of the cascaded GEM. The structural improvement scheme for the effective gain of a single GEM ($G_{eff} = \varepsilon \times G_{abs}$, where ε is collection efficiency) needs to be further studied.

Meanwhile, the methods of fabricating GEMs are mainly divided into two forms. One is micro-hole processing by photolithography and etching. The other is to drill holes on an all-metal surface substrate. The former has the problem of displacement of the openings between the dielectric structure and the metal layer due to the alignment accuracy, while the latter makes it easy to form metal burrs at the opening during drilling, resulting in tip discharge. Representatively, the University of Tokyo and HOYA corporation [28–30] have conducted long-term and in-depth research on the process and performance evaluation of glass GEM. Their processes are all based on specific doped photosensitive etchings glass (such as PEG and PEG3C), and a process similar to the lift-off method is used in the metal deposition step. The via drilling process that relies entirely on photolithography faces two major challenges: First, uneven doping leads to rough hole walls, which manifest as tip structures in the holes, especially at the hole orifices, and there is a greater risk of introducing tip discharges. Second, etching processes that rely on the photosensitive properties of special doped materials (such as Ag) cannot be applied to other glass materials (such as low-background, high-dielectric-strength quartz). In addition, processes such as lift-off will also bring curling that is difficult to eliminate, which is another important factor that increases the risk of tip discharge. Therefore, how to avoid the above problems and form a GEM witha high collection efficiency and tip-less structure is the focus of this paper.

This paper presents an optimized thick GEM (which is collectively referred to as GEM below) structure design model based on the glass processing capability and simulations of the relationship between different hole types, diameters, and the electric field strength. A novel GEM processing method is proposed to solve the technical problem of complete coincidence of the tip-less structural metal opening and hole for double-sided metallization of flat panels with high-density through-hole arrays. A glass GEM with a size of 10 cm × 10 cm was obtained. The electron trajectory over the GEM was constructed and the electrical transparency was obtained according to the statistical distribution of electron locations. Avalanche probabilities were discussed based on region coverage and electron energy.

2. Structure Design and Simulation

The main characterization indicators for GEM are collection efficiency and gain. Previous studies [1–11,16–30] have done a lot of work on how to increase the gain of the detector, and conducted a relatively comprehensive discussion from the aspects of simulation methods, structural design, and loading methods. Therefore, this research focuses on improving the optical transparency and electrical transparency of a single GEM, and conducts exploratory work on the collection efficiency, structural design, and process research.

Optical transparency is the ratio of the area of the GEM surface not covered by metal to the total surface area. This index is positively correlated with the detection position resolution ability. A higher positional resolution can be achieved by increasing the hole density of the micro-holes. As shown in Figure 1, the optical transparency of the two most common types of hole arrangements can be expressed as follows:

$$\varepsilon_{op\_hex} = \frac{2\pi R^2}{\sqrt{3}(2R + D)^2} \tag{1}$$

and

$$\varepsilon_{op\_rect} = \frac{\pi R^2}{(2R + D)^2}, \tag{2}$$

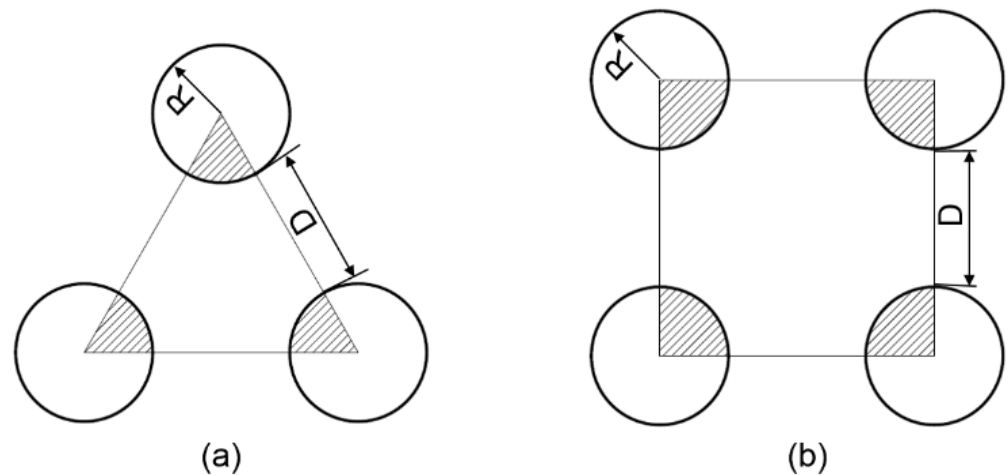where the R is the radius of the hole and D is the pitch.

Figure 1. Basic periodic elements for two conventional hole array arrangements in GEMs. The shaded area is the effective optical transparency area in a basic element. (**a**) A hexagonal element. (**b**) A rectangle element.

It can be inferred that the hexagonal symmetry has a higher proportion of hole density than the rectangle symmetry if the size of the opening and pitch are the same, which means that it has a higher optical transparency than the rectangle. Therefore, we chose a hexagonal symmetrical hole array arrangement in our design.

The electrical transparency evaluates the ratio of the electric field lines passing through the holes to those that terminate at the GEM surface electrodes and hole sides, which is determined by the hole types and the antitype area (the surface area where the field lines fall on). For the antitype area, it can be improved by adjusting the bias voltage after the overall structure is determined. For hole types, sidewalls intersecting the charge path lead to charge accumulation, affecting the collection rate of the total charge consisting of directly collected and induced charges.

The hole formed in processing can be classified into three types: straight, conical, and double conical holes (as shown in Figure 2a–c). These three types were modeled and the same bias voltage is loaded on both of the GEM surfaces for the electric field simulation. Figure 2d–f shows the distribution of field lines under different hole types. The results show that for the same voltage, some of the electric field lines of the latter two hole types terminate on the hole wall. That is to say, electrons entering those two hole structures are more likely to be adsorbed by hitting the hole walls than electrons entering a straight hole. Therefore, it can be considered that the higher the steepness of the hole, the higher the electrical transparency.
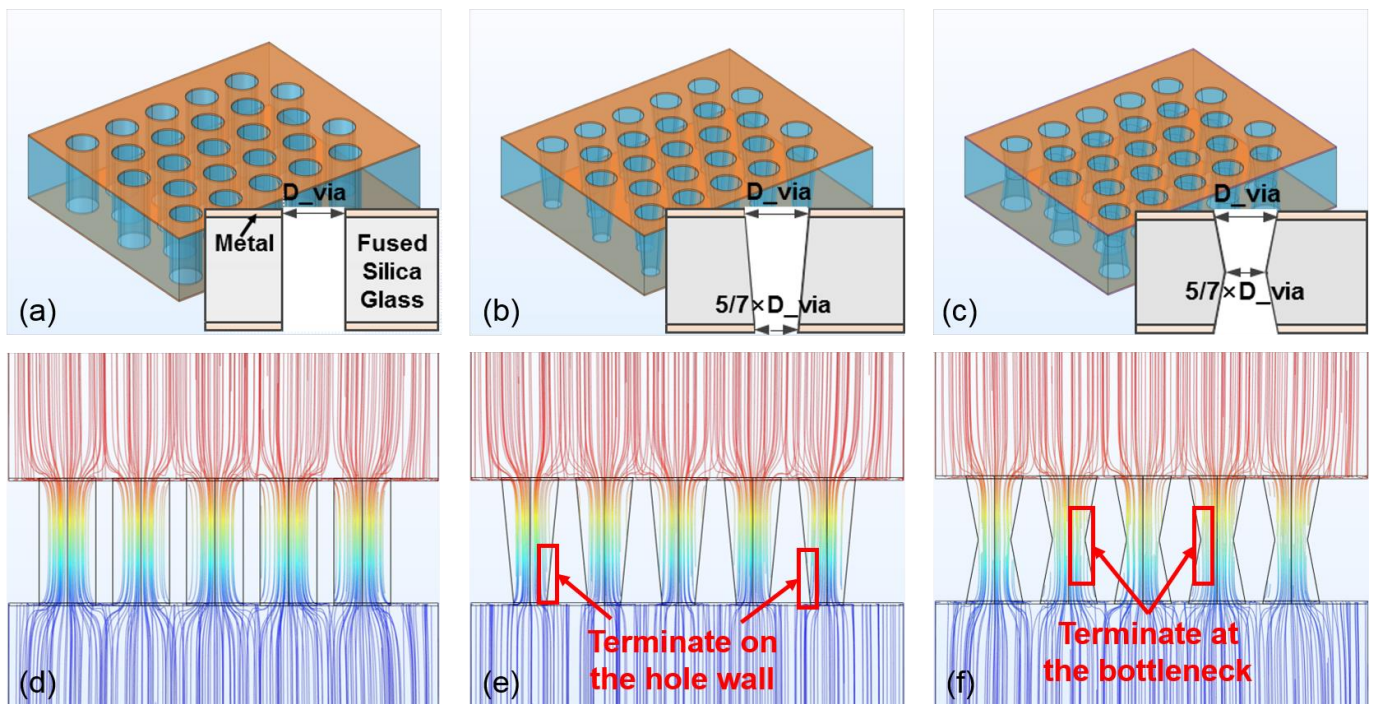
Figure 2. Electric field simulations for different hole structures. Different colors represent different electric potentials. (**a**–**c**) Three different hole structures: (**a**) straight hole, (**b**) conical hole, and (**c**) double conical hole. (**d**,**e**) The corresponding electric field distributions in holes of different shapes under the same initial loading conditions. Both (**e**,**f**) have electric field lines that terminate at the hole walls, which may cause electron attachment, while in straight holes (**d**), the electric field lines all pass through the TGV, extending from above to below the GEM.

When the thickness of the supporting medium is greater than 300 μm, high-frequency laser drilling can effectively form holes with a high steepness and high straightness. Under this thickness condition, we chose the structure formed by the mature laser drilling process (aperture: 70–100 μm, pitch = 2:1, substrate thickness: 100–500 μm) for the electric field strength analysis. Figure 3 shows the distribution of the electric field strength inside the hole simulated by finite element software. The strength reaches a maximum value at the center of the hole and remains constant, and then along the direction perpendicular to the central axis of the hole the field strength decreases linearly with the decrease in the distance from the hole wall, and the closer to the hole wall, the field strength decreases faster. At the orifice, there is a sharp increase close to the metal−insulator interface with an inflection point. This is considered to be a spontaneous field emission phenomenon due to high-voltage-induced breakdown [31].

In addition, for the same average strength of the applied electric field (E_{ave}, equals the electrode voltage/substrate thickness), as the diameter decreases, the maximum field strength increases, and the distribution range of the constant area remains basically unchanged (as shown in Figure 4). However, when the thickness of the substrate increases, the space where the maximum field strength can be maintained as the hole becomes larger, and the maximum field strength also shows an increasing trend. When the average electric field strength is 10^4 V/cm, after the substrate thickness exceeds 300 μm, as the thickness increases, the maximum field strength value basically remains unchanged.
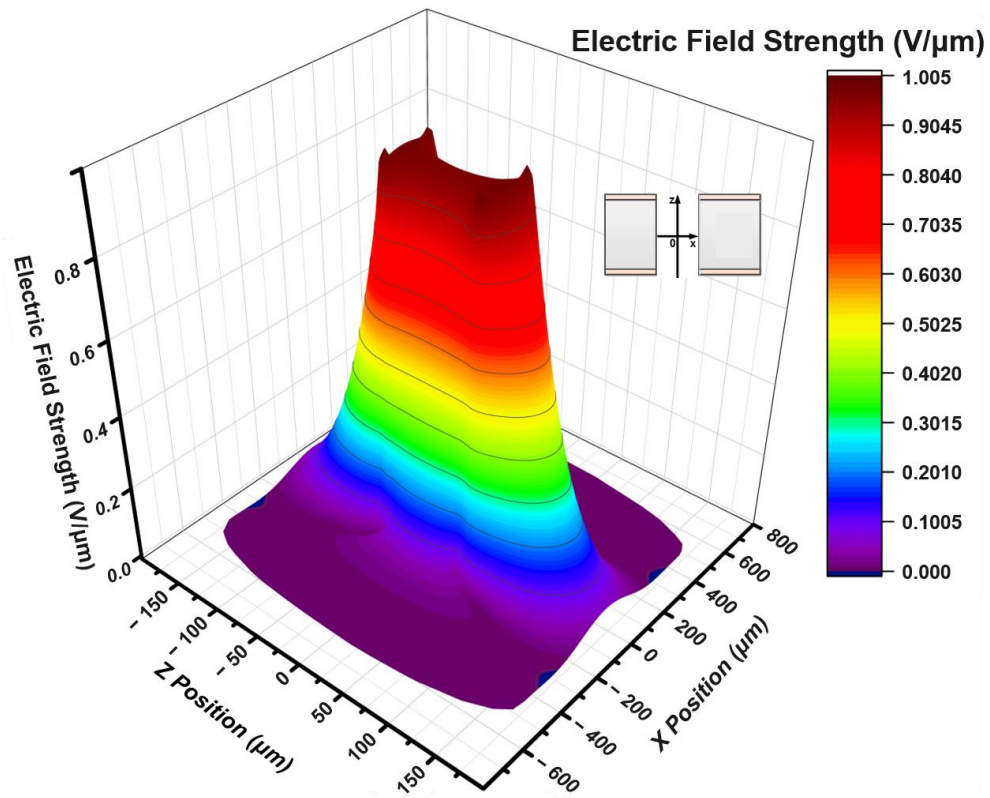
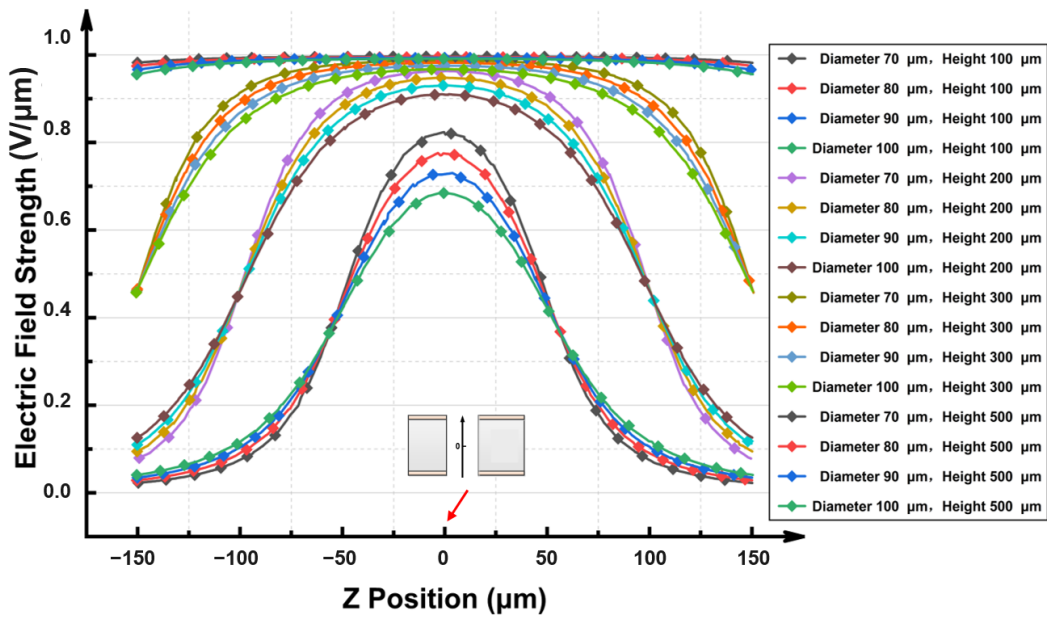**Figure 3.** Simulation of electric field strength in a GEM hole.

Figure 4. Field strength along the line perpendicular to the electrodes passing through the central axis of the hole.
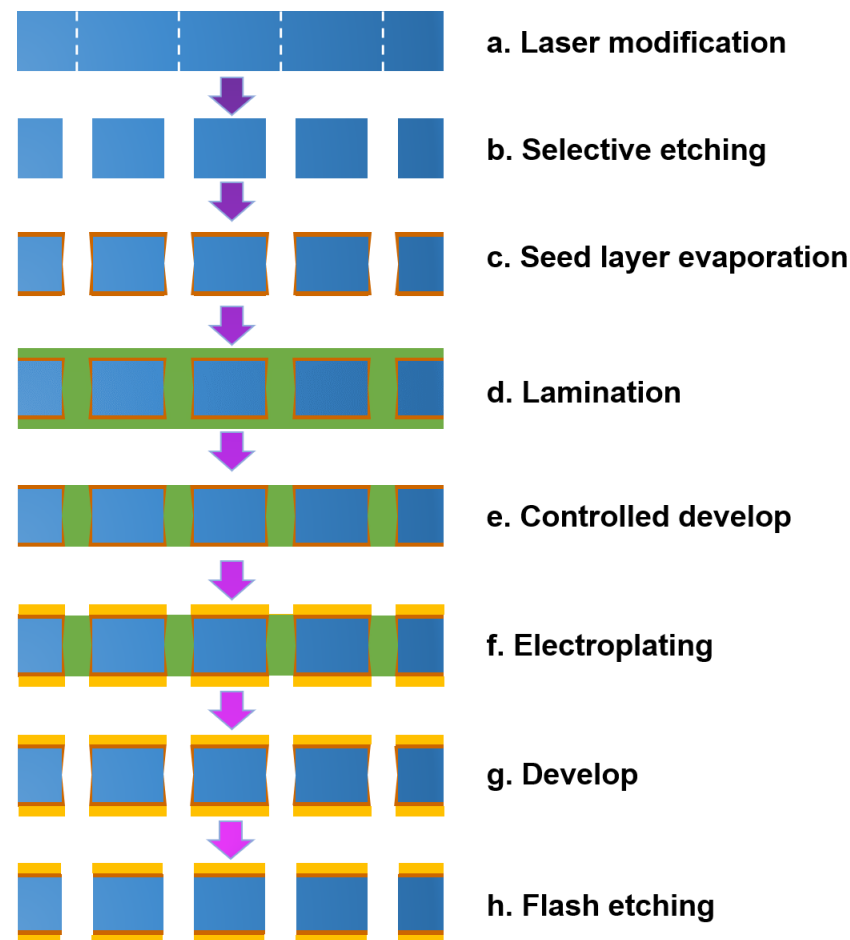
In summary, the parameter settings of the GEM structure in this study are shown in Table 1. The partial model diagram is shown in Figure 2a.

Table 1. Parameter setting of GEM.

Parameter	Description
Size	100 mm × 100 mm
Thickness of Glass (H_G)	300 μm
Thickness of Metal (H_M)	13 μm
Hole diameter (D)	70 μm
Pitch (P)	140 μm
Hole Taper (T)	>89.5°

3. Fabrication Process

There are two main difficulties in GEM manufacturing. On the one hand, the hole shape and position offset would bring more challenges to the alignment capability of the subsequent processes, especially when the number exceeds 100,000 and the area exceeds 100 mm^2. On the other hand, a large area of metal coverage on both surfaces is required while ensuring the insulation of the wall in the holes. Photolithographic processes are applied to pattern the surface metal to align the holes. However, due to conventional lithography alignment requirements, the window of metal opening should be larger than the hole diameter. In addition, the photolithography process is limited by equipment, and a compromise needs to be made between large-format manufacturing requirements and high-precision alignment technology. In this study, a prototype with zero deviation between the hole diameter and metal opening was achieved using advanced laser-induced technology and a novel plugging electroplating technique, without the need for photolithography and machining. The process flow is shown in Figure 5.

a. Laser modification

b. Selective etching

c. Seed layer evaporation

d. Lamination

e. Controlled develop

f. Electroplating

g. Develop

h. Flash etching

Figure 5. Process flow of the glass GEM.

Firstly, laser modification technology is used to form modified regions arranged in arrays on the glass (as shown in Figure 5a). Secondly, holes are formed in the fluoride acid-based etchant at a rate of about 1 μm/s. Thirdly, the PVD (physical vapor deposition) process forms an adhesion layer and a seed layer on the glass substrate. This is followed by lamination and development, as shown in Figure 5d,e. After the photosensitive film is melted and pressed onto the glass substrate, a finely controlled development makes the holes and glass flush on both surfaces. The electroplating of a thicker metal layer on the glass surface is shown in Figure 5f. Finally, after complete development, the thin layer of metal on the hole walls is removed to obtain the GEM structure (as shown in Figure 5h).

3.1. Hole Drilling

A method combining femtosecond laser modification and fluoride acid-based etching was selected for hole formation in order to achieve high perpendicularity and high support substrate thickness. Laser modification is a method that uses ultra-short (<100 fs) laser pulses focused into glass to produce ultra-high localized intensity (>1 kW/cm^2) in a very small space for an ultra-short period of time, resulting in a permanent modification of the material (broken silicon−oxygen bond) [31–33]. By changing the bonding state between the microscopic atoms in the glass, it creates micro-channels with anisotropic high etch selectivity. Hot alkali or fluorine-based solutions are two etchants commonly used in glass etching [34]. A 10% fluorine-based acidic solution was used in our process. Etching can be divided into two main stages. (1) Microvias with a high aspect ratio (size of opening <5 μm) are etched in the local modification area with a selectivity ratio of about 1000. (2) Isotropic porosity expansion under high solution exchange rate conditions. The glass substrate would lose a thickness slightly smaller than the hole diameter during this step.

Figure 6 shows the sample formed after etching. The steepness of the hole is greater than 89.6°, and the positioning accuracy is ±2.5 μm and the orifice is smooth and tip-less.
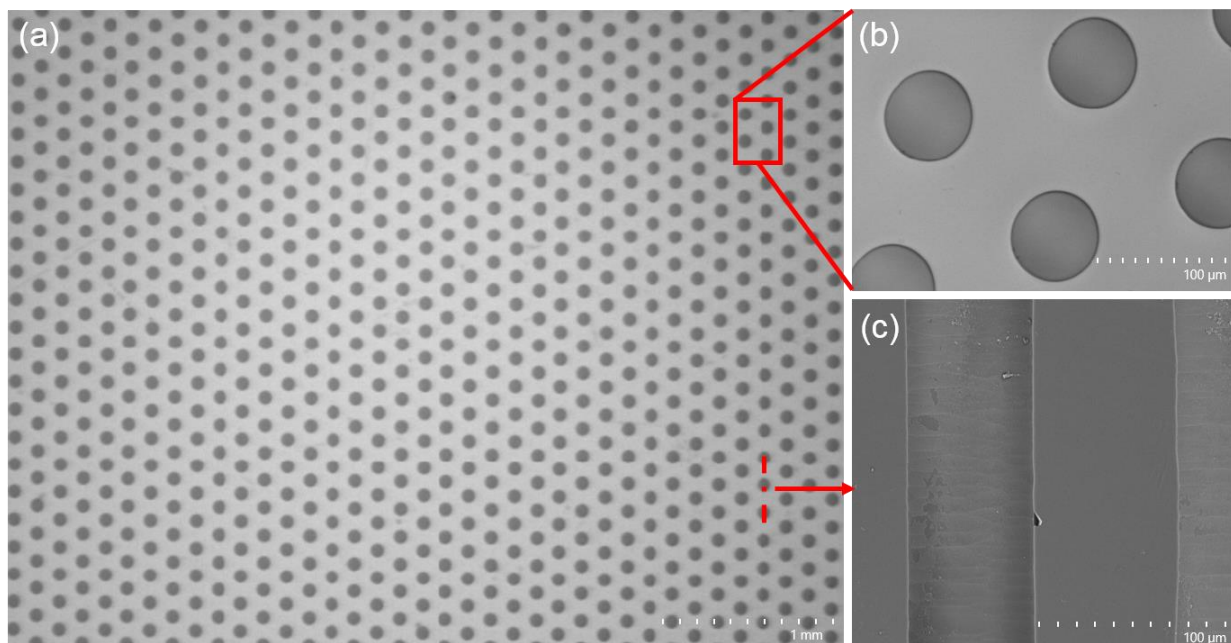

Figure 6. Hole array sample picture. (**a**) A highly consistent hole array taken by the second element equipment. (**b**) An enlarged view of a basic element of the hole array by optical microscope. (**c**) A cross-section of the hole captured by SEM (scanning electron microscope).

3.2. Metal Layer Formation

Because of the characteristics of the hole-forming laser, vertical holes can only be processed on bare glass substrates (also known as via-first). Wafers with a large hole diameter through holes cannot be effectively adsorbed on the spinner plate. In addition, photoresist

may pass through the holes and contaminate the pump. Therefore, a spin-coating process cannot be used. If roll lamination is used, when the hole density is high, the phenomenon of film falling caused by the expansion of air bubbles around the holes will occur.

Therefore, vacuum-laminated polyimide film (PI) was used for hole plugging. Figure 4c–f shows the process of the surface metal patterning. Taking advantage of the coverage of PI material on the metal inside the hole, the surface metal thickness was increased by electroplating. Then, the PI and the seed layer inside the hole were removed by development and flash etching. In this way, a GEM structure with full metal coverage on the surface and insulation inside the holes was formed.

Figure 7 shows the sample formed during the process. Evaporation was selected during the deposition of the seed layer to reduce the coverage of the seed layer on the inside wall of the holes. A seed layer (Ti/Cu) with a surface thickness of approximately 100 nm and a sidewall thickness of less than 50 nm was achieved (as shown in Figure 7a). After vacuum lamination (Figure 7b), a horizontal line of Na_2CO_3 was used to develop the polyimide (as shown in Figure 7c). This process was finely controlled, and the organic film on the surface was completely removed while ensuring that the filling in the holes was still there. Then, after electroplating for 90 min, development and flash etching were performed.
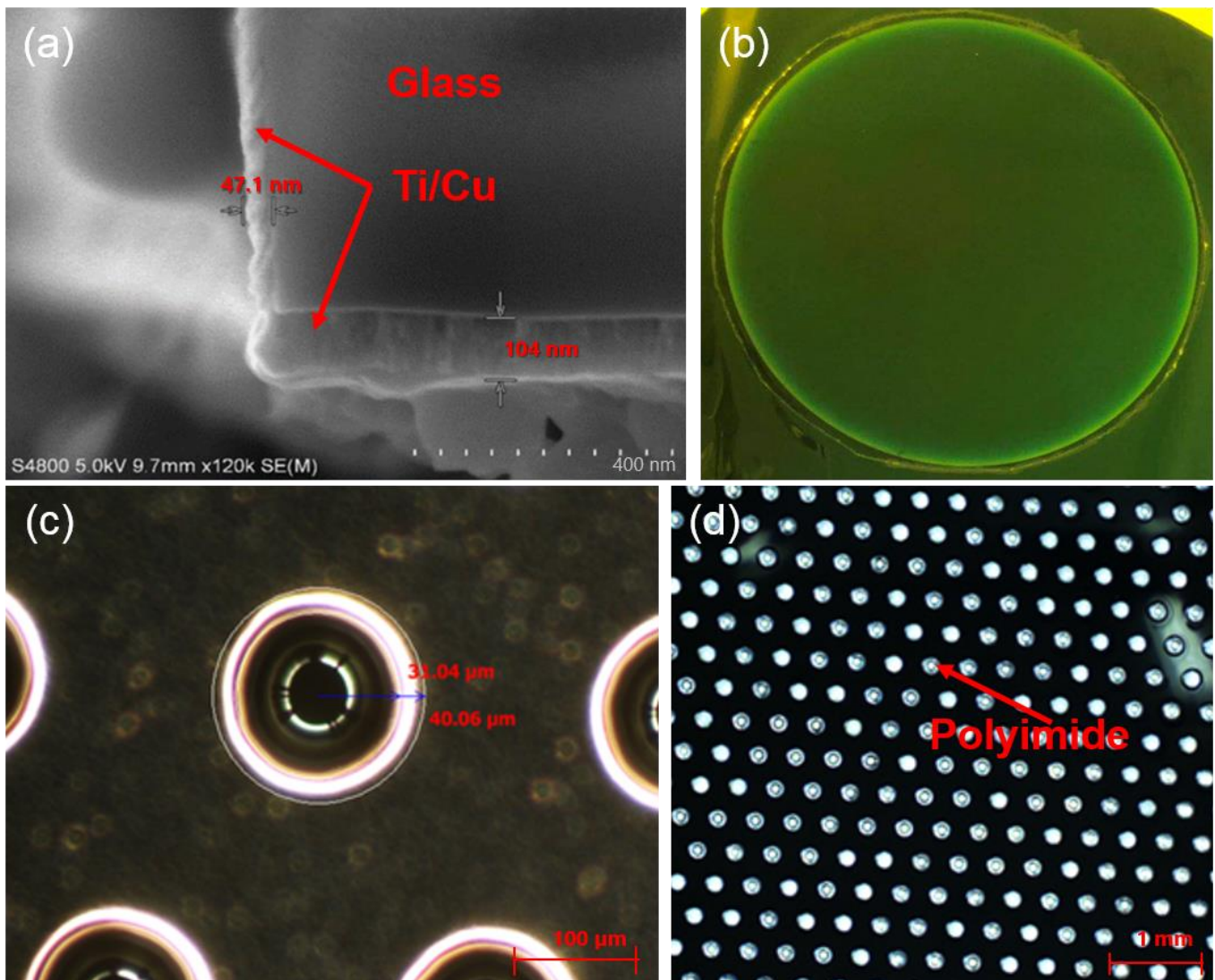

Figure 7. GEM fabrication process. (**a**) SEM picture of the seed layer after sputtering. (**b**) Picture of the sample after vacuum lamination. (**c**) Photographs taken after controlled development. (**d**) Picture observed after plating.

4. Results and Discussion

A glass gas electron multiplier prototype was achieved, which is shown in Figure 8. The effective functional area size was 10 cm × 10 cm. The hole size was about 70 μm. The thickness of the glass substrate was reduced from 310 μm to 240 μm due to thickness loss during hole formation. There was no offset between the position of the glass hole and the metal opening, and the ends of the metals were rounded (as shown in Figure 8b), which is an expected structure for a low probability of discharge.
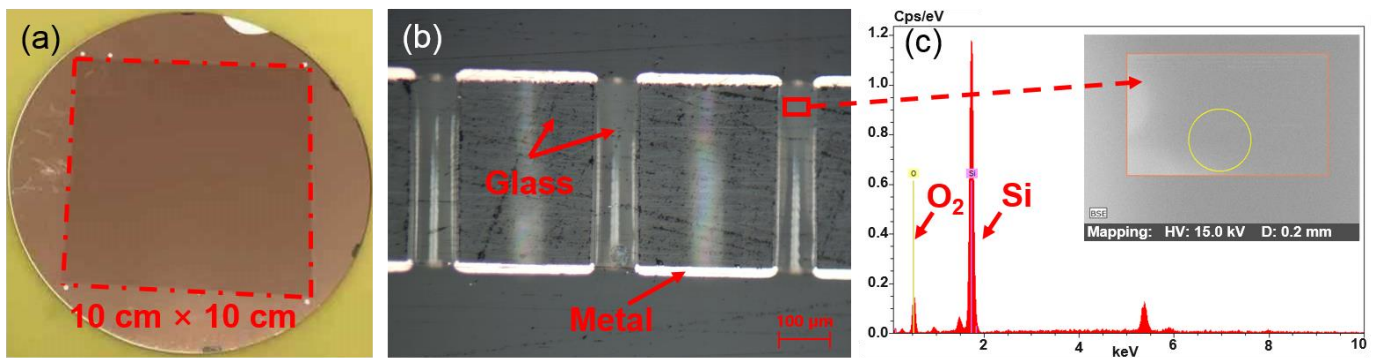

Figure 8. GEM prototype (**a**) Photograph of the GEM sample, where 10 cm × 10 cm is the effective functional area. (**b**) Cross-sectional view of the sample by an optical microscope. (**c**) In-hole composition detection by EDS (energy dispersive spectroscopy).

The ability to finely control the process is key to producing high-quality samples. In addition to fine control during the development of the photosensitive material, the final step used a wet etch on the walls of the holes. Different from the ion exchange rate as the main influencing factor in the small-aperture hole etching process, the key influencing factor of this structure was the reaction rate. Therefore, the control of the particle concentration and time parameters can affect the etching effect in the hole. Over-etching will cause the chemical solution to penetrate into the gap between the surface metal and the glass, resulting in poor reliability or even peeling off of the large-area metal-clad structure, while under-etching will cause metal residues in the holes, resulting in a decline in the performance of the glass GEM. Therefore, the material composition was analyzed at the hole wall near the selected orifice, with no metal residues (as shown in Figure 8c). It can be seen from the cross-sectional view that the metal on the bottom surface protruded about 6 μm from the aperture. This was caused by inconsistency in the development rate of the front and back sides during the first development, and it was necessary to optimize the parameters of the horizontal line device for a better batch.

GEM, as a solid and high-modulus structure, is proposed to replace the multi-wires in TPC (time projection chambers) as an important part of the readout module. This scheme has been widely proposed and studied in a large number of physical simulations [6–8,21,35]. Because of the long period of TPC experimental environment construction, signal and model extraction and analysis, and strong discipline specialization, simulation has been proposed as a means of technical evaluation. In terms of assessing electrical transparency, previous studies [11,35] have used electric field lines to describe the position of electrons. The distribution and counting statistics of electrons on a specified plane is not intuitive enough. If the electrons drifts and lands on the top surface, the signal it was supposed to trigger is lost. Therefore, for the prototype morphology, we simulated the trajectories of electrons above the GEM in a 3D model by loading an electrostatic field-based particle tracking module.

As the TPC size (both diameter and height > 1000 mm) is designed to be much larger than the GEM size (10 cm × 10 cm), the electric field distribution is almost uniform, except for the region near the wall, and the attenuation positions appear randomly; the application of GEM in a TPC is simulated by ignoring the edge effect of the detection environment

and extracting part of a simplified structure area for modular simulation. According to the principle of simplification of the central symmetric structure model, the smallest unit could be selected as a hexagonal structure composed of seven holes. The height and the hole configuration were exactly the same as our prototype.

In this study, for the convenience of observation and modeling, the model was defined as a cuboid structure larger than the minimal simplified model, while the size was much smaller than the TPC. The size of the model was 0.84 mm × 0.84 mm × 0.24 mm, and the drift field and induction field strength were 50 V/cm. The top of the model was the cathode, and the bottom was the collection unit at zero potential (as shown in Figure 9a). The GEM bias voltage was 300 V [35–37]. By uniformly releasing 1000 electrons on top of the cavity, the particle distribution results on the surface of the GEM and the top of the collector were obtained, as shown in Figure 9b. The red dots are where the initially released particles are, the blue dots are the distribution of the particles as they reach the upper surface of the GEM. They drifted along the electric field lines into the holes with 100% electrical transparency.
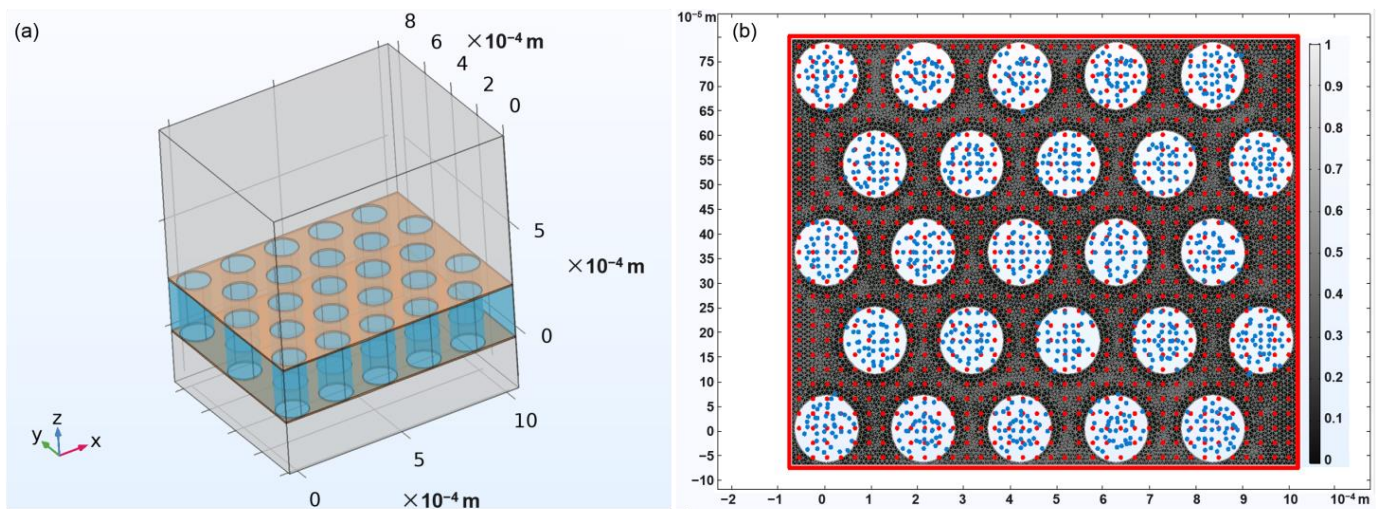

Figure 9. Electron trajectory tracking in a time projection chamber. (**a**) A simplified cavity structure model extracted from a TPC experimental setup. (**b**) A poincaré map of the particle trajectory. The red dots are the positions where the initially released particles are, the blue dots are the distribution states of the particles when they reach the upper surface of the GEM.

Once an electron collides with molecules with enough energy, an avalanche will be triggered. At normal gas densities, the mean free path between two collisions is about 10^{-3} to 10^{-4} cm, and the dissociative ionization when an avalanche occurs is about 30 to 35 eV [36,38]. So, it can be inferred that the avalanche threshold in a GEM is at least 3×10^4 V/cm [39].

Taking the formed GEM structure parameters as the input conditions, the kinetic energy of electrons without avalanche caused by collision was evaluated, and the motion state analysis was performed with the avalanche threshold as the boundary. In the drift field, the electric field strength is low, and the position and initial velocity of electrons are random, so this paper did not discuss the calculation model of the particle trajectory reconstruction. Decoupling from the above model, the electron velocity in a certain region was related to the electric field strength. Therefore, at a normal xenon gas density (1 Torr), the electron velocity in our model could be ideally set as the product of 2×10^5 cm^2/s·V [40] and the electric field strength. The energy of the electrons in z direction is shown in Figure 10.

It can be seen from the figure that the change trend in charge energy and electric field strength is basically the same. In the edge region, due to the unequal electric field force and gas resistance, the kinetic energy of electrons is in a state of rapid change. When the field strength in the hole is stable, the electric force equals the gas resistance, and the

electron velocity reaches the maximum and is maintained. When the voltage is greater than 50 V, the kinetic energy of the electrons in the holes can be higher than 30 eV, which has the conditions to cause an avalanche effect. The avalanche region is located in the hole approximately 25 μm from the opening. When the voltage reaches 100 V or even higher, an avalanche occurs within a certain distance outside the hole. The higher the voltage, the farther the avalanche start and end interfaces are from the orifice. According to this condition, the optimal placement position of the induction pads can be judged.
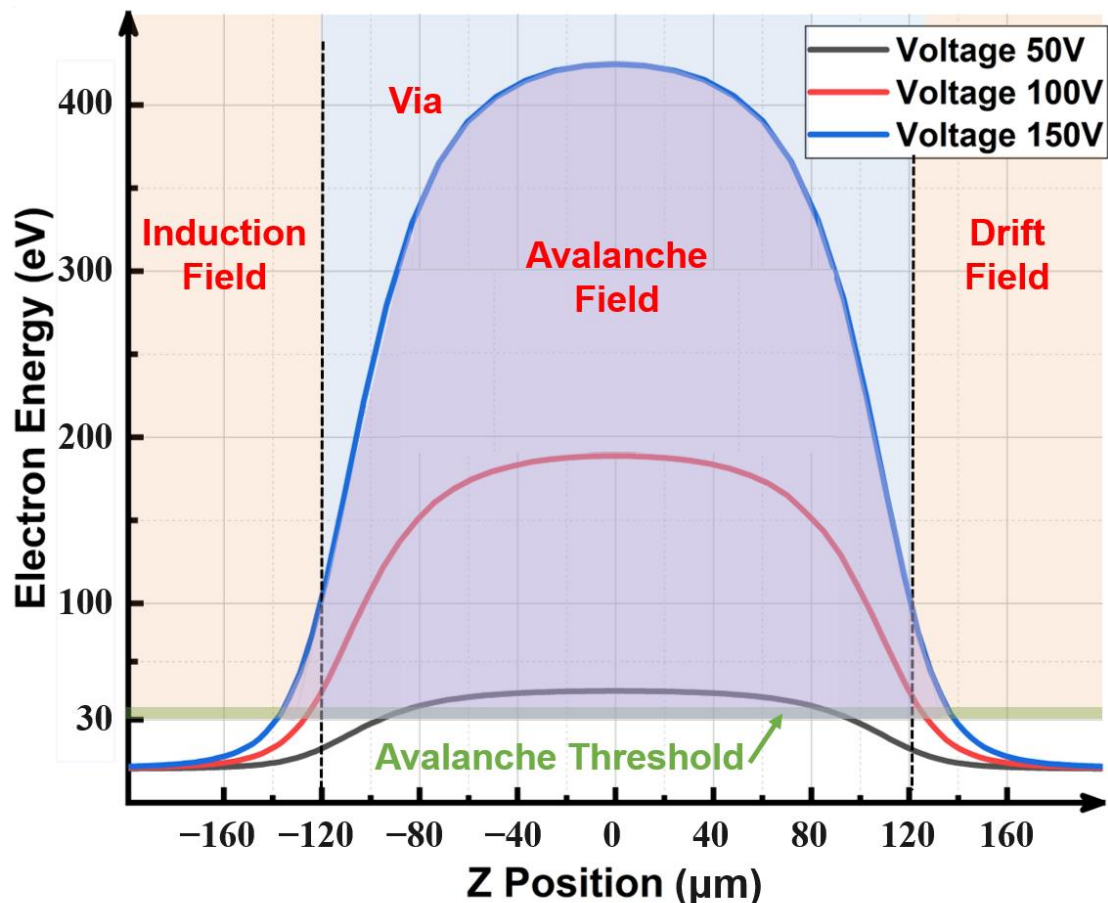

Figure 10. Electron energy in holes.

5. Conclusions

This paper describes the formation of thick glass GEMs from both design and process aspects. From the perspective of transparency, it analyzes and discusses the design method of GEM. The prototype was fabricated by combining an advanced glass hole formation process with an innovative selective metallization process method. This process changes the traditional processing method that requires photolithography, improves precision, and reduces the cost of patterning processing of high-density hole array samples.

The detailed fabrication process is described. A large number of holes are formed at one time, with a high consistency and smooth morphology, which is the structure required for high resolution and low discharge probability applications. It is proposed to completely fill the hole with a photosensitive film. It solves the problem of the limitation that laser modification can only be used for raw glass without pretreatment.

Furthermore, the new process proposed in this paper is highly compatible with hetero structures (e.g., simultaneous metallization of multi-structured holes). It can also be applied to the processing of MEMS and semiconductor microstructures, especially those with large diameter holes.

Finally, this paper attempts to propose a compromise approach to shorten the iterative optimization cycle between the semiconductor domain and the high-energy detection domain. The prototype-based particle trajectory tracking and statistical simulation of state provide new ideas for evaluating GEMs.

Author Contributions: Conceptualization, X.W., X.S., L.C. and Q.W.; data curation, X.W. and Q.W.; formal analysis, X.W.; investigation, X.W., X.S. and Q.W.; methodology, X.W.; project administration, Q.W.; supervision, L.C. and Q.W.; validation, X.W.; writing—original draft, X.W.; writing—review and editing, Q.W. All authors have read and agreed to the published version of the manuscript.

Data Availability Statement: Not applicable.

Conflicts of Interest: The authors declare no conflict of interest.

References

1. Sauli, F. Gem: A New Concept for Electron Amplification in Gas Detectors. *Nucl. Instrum. Methods Phys. Res. Sect. A Accel. Spectrometers Detect. Assoc. Equip.* **1997**, *386*, 531–534. [CrossRef]
2. Bachmann, S.; Kappler, S.; Ketzer, B.; Ropelewski, L.; Schulte, E.; Müller, T.; Sauli, F. High Rate X-ray Imaging Using Multi-Gem Detectors with a Novel Readout Design. *Nucl. Instrum. Methods Phys. Res. Sect. A Accel. Spectrometers Detect. Assoc. Equip.* **2002**, *478*, 104–108. [CrossRef]
3. Guedes, G.P.; Breskin, A.; Chechik, R.; Vartsky, D.; Bar, D.; Barbosa, A.F.; Marinho, P.R.B. Two-Dimensional Gem Imaging Detector with Delay-Line Readout. *Nucl. Instrum. Methods Phys. Res. Sect. A Accel. Spectrometers Detect. Assoc. Equip.* **2003**, *513*, 473–483. [CrossRef]
4. Linczuk, P.; Poźniak, K.; Chernyshova, M. Soft Real-Time Data Processing Solutions in Measurement Systems on Example of Small-Scale Gem Based X-ray Spectrometer. In *Photonics Applications in Astronomy, Communications, Industry, and High Energy Physics Experiments*; SPIE: Bellingham, WA, USA, 2022.
5. Caruggi, F.; Cancelli, S.; Celora, A.; Guiotto, F.; Croci, G.; Tardocchi, M.; Murtas, F.; Oliveira, R.; Cippo, E.P.; Gorini, G. Performance of a Triple Gem Detector Equipped with Al-Gem Foils for X-rays Detection. *Nucl. Instrum. Methods Phys. Res. Sect. A Accel. Spectrometers Detect. Assoc. Equip.* **2023**, *1047*, 167855. [CrossRef]
6. Kaminski, J.; Ball, M.; Bieser, F.; Janssen, M.; Kappler, S.; Ledermann, B.; Müller, T.; Ronan, M.; Wienemann, P. Development and Studies of a Time Projection Chamber with Gems. *Nucl. Instrum. Methods Phys. Res. Sect. A Accel. Spectrometers Detect. Assoc. Equip.* **2004**, *535*, 201–205. [CrossRef]
7. Sauli, F. *Micro-Pattern Gaseous Detectors: Principles of Operation and Applications*; World Scientific: Singapore, 2020.
8. Dangendorf, V.; Laczko, G.; Reginatto, M.; Vartsky, D.; Goldberg, M.; Mor, I.; Breskin, A.; Chechik, R. Detectors for Time-of-Flight Fast-Neutron Radiography 1. Neutron-Counting Gas Detector. *Nucl. Instrum. Methods Phys. Res. Sect. A Accel. Spectrometers Detect. Assoc. Equip.* **2005**, *542*, 197–205. [CrossRef]
9. Ahmed, A.; Kumar, A.; Naimuddin, M.; Babij, M.; Bielowka, P. The Qualification of Gem Detector and Its Application to Imaging. *J. Instrum.* **2022**, *17*, P04002. [CrossRef]
10. Shalem, C.; Chechik, R.; Breskin, A.; Michaeli, K. Advances in Thick Gem-Like Gaseous Electron Multipliers—Part I: Atmospheric Pressure Operation. *Nucl. Instrum. Methods Phys. Res. Sect. A Accel. Spectrometers Detect. Assoc. Equip.* **2006**, *558*, 475–489. [CrossRef]
11. Chechik, R.; Breskin, A.; Shalem, C.; Mormann, D. Thick Gem-Like Hole Multipliers: Properties and Possible Applications. *Nucl. Instrum. Methods Phys. Res. Sect. A Accel. Spectrometers Detect. Assoc. Equip.* **2004**, *535*, 303–308. [CrossRef]
12. Adhikari, G.; Kharusi, S.A.; Angelico, E.; Anton, G.; Arnquist, I.J.; Badhrees, I.; Bane, J.; Belov, V.; Bernard, E.P.; Bhatta, T.; et al. Nexo: Neutrinoless Double Beta Decay Search Beyond 10^{28} Year Half-Life Sensitivity. *Nucl. Part. Phys.* **2021**, *49*, 015104. [CrossRef]
13. Leonard, D.S.; Grinberg, P.; Weber, P.; Baussan, E.; Djurcic, Z.; Keefer, G.; Piepke, A.; Pocar, A.; Vuilleumier, J.-L.; Vuilleumier, J.-M.; et al. Systematic Study of Trace Radioactive Impurities in Candidate Construction Materials for Exo-200. *Nucl. Instrum. Methods Phys. Res. Sect. A Accel. Spectrometers Detect. Assoc. Equip.* **2008**, *591*, 490–509. [CrossRef]
14. Albert, J.B.; Anton, G.; Arnquist, I.J.; Badhrees, I.; Barbeau, P.; Beck, D.; Belov, V.; Bourque, F.; Brodsky, J.P.; Brown, E.; et al. Sensitivity and Discovery Potential of the Proposed Nexo Experiment to Neutrinoless Double-B Decay. *Phys. Rev. C* **2018**, *97*, 065503. [CrossRef]
15. Arnquist, I.J.; Beck, C.; Vacri, M.L.; Harouaka, K.; Saldanha, R. Ultra-Low Radioactivity Kapton and Copper-Kapton Laminates. *Nucl. Instrum. Methods Phys. Res. Sect. A Accel. Spectrometers Detect. Assoc. Equip.* **2020**, *959*, 163573. [CrossRef]
16. Amaro, F.D.; Roque, R.; Duarte, N.V.; Cortez, A.; Mir, J.A. Operation of a Novel Large Area, High Gain, Single Stage Gaseous Electron Multiplier. *J. Instrum.* **2021**, *16*, P01033. [CrossRef]

17.　Patra, R.N.; Singaraju, R.N.; Dalal, S.; Biswas, S.; Viyogi, Y.P.; Nayak, T.K. Characteristic Study of a Quadruple Gem Detector in Different Electric Field Configurations. *Nucl. Instrum. Methods Phys. Res. Sect. A Accel. Spectrometers Detect. Assoc. Equip.* **2019**, *936*, 433–435. [CrossRef]

18.　Bhattacharyya, R.; Adak, R.P.; Sahu, S.K.; Sahu, P.K. Study of Efficiency and Gain Uniformity at Different Gas Flow Rates of a Quad-Gem Detector. *J. Instrum.* **2022**, *17*, P10008. [CrossRef]

19.　Lukas, L.; Fabbietti, L.; Gasik, P.; Klemenz, T. High Voltage Scheme Optimization for Secondary Discharge Mitigation in Gem-Based Detectors. *J. Instrum.* **2019**, *14*, P08024.

20.　Mohamed, S.; Elkafrawy, T.; Merlin, J.A. Reduction of High Voltage Discharge in Gem Detectors for the Me0 Station of the Cms Forward Muon System. In Proceedings of the Tenth Annual Large Hadron Collider Physics (LHCP2022), Online, 16–20 May 2022.

21.　Fedorchuk, O. *Investigations of the Long-Term Stability of a Gas Electron Multipliers and Double Hit Resolution for the Highly Granular Time-Projection Chamber*; Staats-und Universitätsbibliothek Hamburg Carl von Ossietzky: Hamburg, Germany, 2019.

22.　Utrobicic, A.; Kovacic, M.; Erhardt, F.; Jercic, M.; Poljak, N.; Planinic, M. Studies of the Delayed Discharge Propagation in the Gas Electron Multiplier (Gem). *Nucl. Instrum. Methods Phys. Res. Sect. A Accel. Spectrometers Detect. Assoc. Equip.* **2019**, *940*, 262–273. [CrossRef]

23.　Bachmann, S.; Bressan, A.; Capeáns, M.; Deutel, M.; Kappler, S.; Ketzer, B.; Polouektov, A.; Ropelewski, L.; Sauli, F.; Schulte, E. Discharge Studies and Prevention in the Gas Electron Multiplier (Gem). *Nucl. Instrum. Methods Phys. Res. Sect. A Accel. Spectrometers Detect. Assoc. Equip.* **2002**, *479*, 294–308. [CrossRef]

24.　Bianco, M.; Fallavollita, F.; Fiorina, F.; Maggi, M.; Pellecchia, A.; Garcia, L.F.R.; Rosi, N.; Verwilligen, P. High Rate Capability Studies of Triple-Gem Detectors for the Me0 Upgrade of the Cms Muon Spectrometer. *J. Instrum.* **2022**, *17*, C02009. [CrossRef]

25.　Fallavollita, F. Triple-Gas Electron Multiplier Technology for Future Upgrades of the Cms Experiment: Construction and Certification of the Cms Ge1/1 Detector and Longevity Studies. Ph.D. Thesis, University of Pavia, Pavia, Italy, 2019.

26.　Ketzer, B.; Altunbas, M.C.; Dehmelt, K.; Ehlers, J.; Friedrich, J.; Grube, B.; Kappler, S.; Konorov, I.; Paul, S.; Placci, A. Triple Gem Tracking Detectors for Compass. *IEEE Trans. Nucl. Sci.* **2002**, *49*, 2403–2410. [CrossRef]

27.　Buzulutskov, A.; Breskin, A.; Chechik, R.; Garty, G.; Sauli, F.; Shekhtman, L. Further Studies of the Gem Photomultiplier. *Nucl. Instrum. Methods Phys. Res. Sect. A Accel. Spectrometers Detect. Assoc. Equip.* **2000**, *442*, 68–73. [CrossRef]

28.　Fujiwara, T.; Mitsuya, Y.; Takahashi, H. Radiation Imaging with Glass Gas Electron Multipliers (G−Gems). *Nucl. Instrum. Spectrometers Methods Phys. Res. Sect. A Accel. Detect. Assoc. Equip.* **2018**, *878*, 40–49. [CrossRef]

29.　Tokanai, F.; Moriya, T.; Takeyama, M.; Sakurai, H.; Gunji, S.; Fushie, T.; Kikuchi, H.; Sumiyoshi, T.; Sugiyama, H. Novel Glass Ceramic-Type Micropattern Gas Detector with Peg3c. *Nucl. Instrum. Spectrometers Methods Phys. Res. Sect. A Accel. Detect. Assoc. Equip.* **2013**, *732*, 273–276. [CrossRef]

30.　Mitsuya, Y.; Fujiwara, T.; Fushie, T.; Maekawa, T.; Takahashi, H. Development of Large-Area Glass Gem. *Nucl. Instrum. Spectrometers Methods Phys. Res. Sect. A Accel. Detect. Assoc. Equip.* **2015**, *795*, 156–159. [CrossRef]

31.　Gamaly, E.G.; Rode, A.V. Physics of Ultra-Short Laser Interaction with Matter: From Phonon Excitation to Ultimate Transformations. *Prog. Quantum Electron.* **2013**, *37*, 215–323. [CrossRef]

32.　Tuennermann, A.; Nolte, S.; Limpert, J. Femtosecond Vs. Picosecond Laser Material Processing: Challenges in Ultrafast Precision Laser Micromachining of Metals at High Repetition Rates. *Laser Tech. J.* **2010**, *7*, 34–38. [CrossRef]

33.　Ostholt, R.; Ambrosius, N.; Krüger, R.A. High Speed through Glass Via Manufacturing Technology for Interposer. In Proceedings of the 5th Electronics System-Integration Technology Conference (ESTC) 2014, Helsinki, Finland, 16–18 September 2014.

34.　Bellouard, Y.; Said, A.; Dugan, M.; Bado, P. Fabrication of High-Aspect Ratio, Micro-Fluidic Channels and Tunnels Using Femtosecond Laser Pulses and Chemical Etching. *Opt. Express* **2004**, *12*, 2120–2129. [CrossRef]

35.　Sauli, F.; Ropelewski, L.; Everaerts, P. Ion Feedback Suppression in Time Projection Chambers. *Nucl. Instrum. Methods Phys. Res. Sect. A Accel. Spectrometers Detect. Assoc. Equip.* **2006**, *560*, 269–277. [CrossRef]

36.　Christophorou, L.G.; Olthoff, J.K.; Rao, M.V.V.S. Electron Interactions with Cf4. *J. Phys. Chem. Ref. Data* **1996**, *25*, 1341–1388. [CrossRef]

37.　Christophorou, L.G.; Olthoff, J.K. Electron Interactions with Plasma Processing Gases: An Update for Cf4, Chf3, C2f6, and C3f8. *J. Phys. Chem. Ref. Data* **1999**, *28*, 967–982. [CrossRef]

38.　Mohapatra, A.D.; Moulik, T. *Role of CF4 in Gas Amplification in Gems*; National Institute of Science Education and Research: Khurda, India, 2011.

39.　Blum, W.; Rolandi, L. *Particle Detection with Drift Chambers*; Springer Science & Business Media: Berlin/Heidelberg, Germany, 2008.

40.　Dias, T.H.V.T.; Stauffer, A.D.; Cone, C.A.N. A Unidimensional Monte Carlo Simulation of Electron Drift Velocities and Electroluminescence in Argon, Krypton and Xenon. *J. Phys. D Appl. Phys.* **1986**, *19*, 527. [CrossRef]